Disclinations in square and hexagonal patterns

A. A. Golovin
Department of Engineering Sciences and Applied Mathematics, Northwestern University, Evanston, Illinios 60208-3100

A. A. Nepomnyashchy
Department of Mathematics and Minerva Center for Nonlinear Physics of Complex Systems, Technion, Israel Institute of Technology, Haifa 32000, Israel

(Received 27 February 2002; revised manuscript received 14 February 2003; published 2 May 2003)

We report the observation of defects with fractional topological charges (disclinations) in square and hexagonal patterns as numerical solutions of several generic equations describing many pattern-forming systems: Swift-Hohenberg equation, damped Kuramoto-Sivashinsky equation, as well as nonlinear evolution equations describing large-scale Rayleigh-Benard and Marangoni convection in systems with thermally nearly insulated boundaries. It is found that disclinations in square and hexagonal patterns can be stable when nucleated from special initial conditions. The structure of the disclinations is analyzed by means of generalized Cross-Newell equations.

DOI: 10.1103/PhysRevE.67.056202 PACS number(s): 45.70.Qj, 47.54.+r, 89.75.Kd

I. INTRODUCTION

Topological defects in condensed- and soft-matter systems are ubiquitous and very interesting objects [1,2]. In particular, they are often observed in systems exhibiting spontaneous formation of spatially regular patterns. The characteristic feature of spatially periodic patterns is that they are characterized by one or more wave vectors and are invariant with respect to the wave vector sign change. In other words, the patterns are characterized by *directors* rather than wave vectors, much like liquid crystals. This makes it possible for special type of point defects with fractional topological charges—*disclinations*—to occur in such patterns.

Disclinations in roll patterns have been observed in several pattern forming systems and have been analyzed by Newell and co-workers [3,4]. The characteristic feature of these defects is that when going around the defect core, one observes the pattern wave vector rotating. It is rotating in such a way that after making a full circle around the core, the wave vector of the roll pattern rotates by $\pm 180°$ so that the roll pattern ''goes back to itself.'' Such a defect can be characterized by a topological charge—the angle of the pattern wave vector rotation around the defect in fractions of 2π. Thus, two types of disclinations in roll patterns, with the minimal fractional topological charge, can be distinguished: a convex disclination, with the topological charge 1/2, and a concave one, with the topological charge $-1/2$. An example of an order parameter field containing a disclination can be constructed in the following way. Out of the disclination core, the roll pattern around the disclination is represented by the order parameter $\sim\cos[\mathbf{k}(\phi)\cdot\mathbf{r}]$, $\mathbf{k}(\phi)=[\mp\sin(\phi/2),\cos(\phi/2)]$, where the signs $\mp$ correspond to a convex and a concave disclination, respectively. In the polar coordinates $x=r\cos\phi$, $y=r\sin\phi$, and therefore a convex disclination in a roll pattern, with the topological charge 1/2, is represented by the order parameter $\sim\cos[r\sin(\phi/2)]$, while a concave disclination in a roll pattern, with the topological charge $-1/2$, is represented by the order parameter $\sim\cos[r\sin(3\phi/2)]$.

Similar types of defects could be expected to exist in square and hexagonal patterns that are observed in many pattern-forming systems such as convection [5], Faraday waves [6], granular materials [7], directional solidification [8], reaction-diffusion systems [9], ferrofluids [10], nonlinear optical systems [11], etc. In the case of a square pattern that is characterized by a mutually orthogonal pair of directors, disclinations with the minimal absolute value of the topological charge correspond to the rotation of the square pattern by $\pm 90°$. In this case, a convex disclination has the topological charge 1/4 and a concave disclination has the topological charge $-1/4$. For these disclinations, the order parameter is $\sim\cos[\mathbf{k}_1(\phi)\cdot\mathbf{r}]+\cos[\mathbf{k}_2(\phi)\cdot\mathbf{r}]$ with $\mathbf{k}_1(\phi)=[\cos(\phi/4),\pm\sin(\phi/4)]$ and $\mathbf{k}_2(\phi)=[\mp\sin(\phi/4),\cos(\phi/4)]$, where the signs $\pm$ correspond to a convex and a concave disclination, respectively. In the polar coordinates, the order parameter is $\sim\cos[r\cos(3\phi/4)]+\cos[r\sin(3\phi/4)]$ for a convex disclination and $\sim\cos[r\cos(5\phi/4)]+\cos[r\sin(5\phi/4)]$ for a concave one. Similarly, in a hexagonal pattern, disclinations with the minimal absolute value of the topological charge correspond to the pattern rotation by $\pm 60°$, with a convex disclination having the topological charge 1/6 and a concave one $-1/6$. The order parameter is $\sim\cos[\mathbf{k}_1(\phi)\cdot\mathbf{r}]+\cos[\mathbf{k}_2(\phi)\cdot\mathbf{r}]+\cos[\mathbf{k}_3(\phi)\cdot\mathbf{r}]$, with $\mathbf{k}_1(\phi)=[\cos(\phi/6),\pm\sin(\phi/6)]$, $\mathbf{k}_2(\phi)=[\cos(\phi/6\pm\pi/3),\pm\sin(\phi/6\pm\pi/3)]$, and $\mathbf{k}_3(\phi)=[\cos(\phi/6\pm 2\pi/3),\sin(\phi/6\pm 2\pi/3)]$, where the signs $\pm$ correspond to a convex and concave disclination, respectively. In the polar coordinates, the order parameter of a convex disclination is thus $\sim\cos[r\cos(5\phi/6)]+\cos[r\cos(5\phi/6+\pi/3)]+\cos[r\cos(5\phi/6+2\pi/3)]$, while a concave disclination has the order parameter $\sim\cos[r\cos(7\phi/6)]+\cos[r\cos(7\phi/6+\pi/3)]+\cos[r\cos(7\phi/6+2\pi/3)]$.

The subject of this paper is to investigate whether disclinations in square and hexagonal patterns can be expected to be observed in pattern-forming systems. Disclinations in square patterns are briefly discussed in Ref. [12] (see also Ref. [13]) from the point of view of defects in a cubic crystal lattice. Also, square patterns resembling disclination struc-

ture were observed in convection in a binary mixture in a circular container [14]. Hexagonal patterns with defects possibly resembling disclinations were observed in experiments with chemical patterns [15] as well as in numerical simulations of some reaction-diffusion systems [16–18]. However, to the best of our knowledge, there has been no systematic investigation of these types of defects in square and hexagonal patterns. In this paper, we study disclinations in square and hexagonal patterns described above by solving numerically several generic nonlinear evolution equations, well known to describe pattern formation in a variety of systems. We demonstrate that the existence of stable stationary disclinations in square and hexagonal patterns is possible in several systems, with both potential and nonpotential dynamics.

II. DISCLINATIONS IN SQUARE PATTERNS

As an example of a pattern-forming system in which a square pattern is selected, we choose Rayleigh-Benard convection in a liquid layer between thermally nearly insulated plates. The nonlinear evolution of this system is described by the following evolution equation [19–21]:

$$\epsilon^2 \frac{\partial T}{\partial t} = \epsilon^2 T - (1+\nabla^2)^2 T + \frac{1}{3}\nabla\cdot(\nabla T|\nabla T|^2), \qquad (1)$$

where T is the mean temperature across the liquid layer. A weakly nonlinear analyzis of this equation near the instability threshold ($\epsilon \ll 1$) predicts the appearance of a square planform [22].

We have performed a numerical simulation of this equation by means of a pseudospectral code with periodic boundary conditions. Our numerical simulations show that indeed, starting from small-amplitude random data, a square pattern, with some defects and domain walls between regions filled with differently oriented squares is formed. In order to examine a possibility for a disclination defect to exist in a square pattern we have solved Eq. (1) numerically, in a large domain with length $L = 80\pi \times 80\pi$, starting from two types of small-amplitude initial conditions discussed above, and corresponding to a convex and a concave disclination with topological charges 1/4 and $-1/4$, respectively. Figure 1 shows a stationary solution of Eq. (1) in the form of a convex disclination with the topological charge 1/4 for $\epsilon^2 = 0.4$. Figure 2 shows a stationary solution of Eq. (1) in the form of a concave disclination with the topological charge $-1/4$ for $\epsilon^2 = 0.1$ [23]. One can see that both of these disclination patterns consist of a core with threefold (Fig. 1) or fivefold (Fig. 2) symmetry and a surrounding square pattern. For larger ϵ, the disclination structure is almost defect free. For smaller ϵ, there is a set of dislocations ''emitted'' from the core (emission of dislocations is observed at small supercriticality for both concave and convex disclinations). Dislocations appear because the pattern has a prescribed wavelength: such a process of ''healing'' disclinations by dislocations was qualitatively described in Ref. [12]. However, it is important that the set of dislocations is *not* continuous in that it does not form a domain boundary separating regions with differently oriented squares, so that when one goes around the core the orientation of squares (the pattern wave vectors) rotates continuously by $\pm\pi/2$.

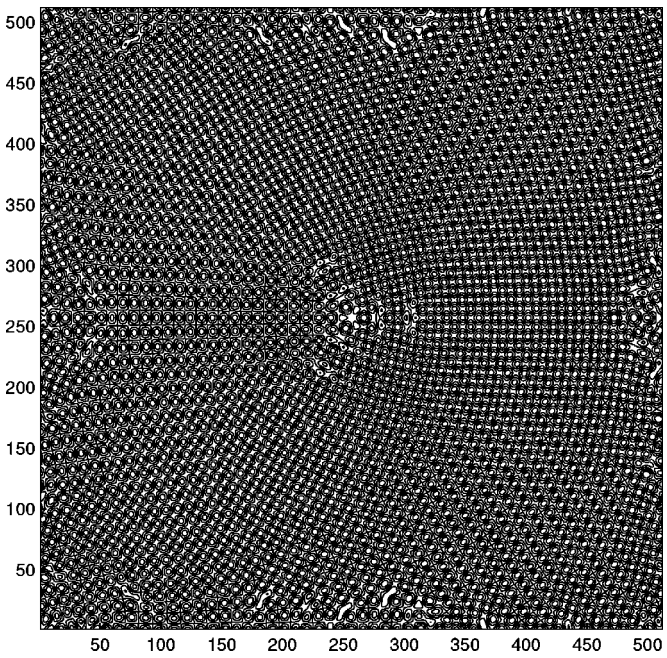

FIG. 1. Stable stationary solutions of Eq. (1) with $\epsilon^2 = 0.4$, forming a convex disclination in a square pattern, with the topological charge 1/4.

The structure of disclinations in a square pattern can be qualitatively understood on the basis of stationary Cross-Newell equations for a square pattern which are similar to the Cross-Newell equations for hexagonal and triangular pat-

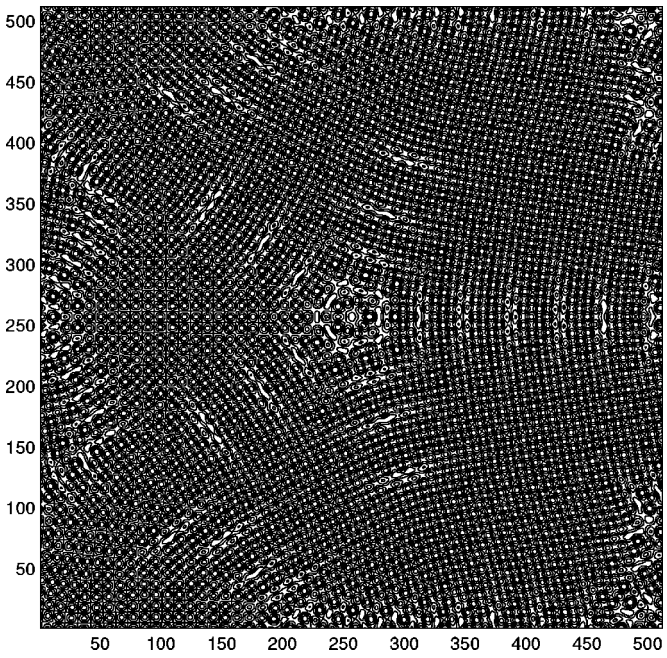

FIG. 2. Stable stationary solutions of Eq. (1) with $\epsilon^2 = 0.1$, forming a concave disclination in a square pattern, with the topological charge $-1/4$.

terns in potential systems derived in Ref. [24]. According to the analysis presented in Ref. [24], a pattern formed in a potential system and based on two local wave vectors (two phases) $\mathbf{k}_1=\nabla\Theta_1$, and $\mathbf{k}_2=\nabla\Theta_2$ is described by the stationary Cross-Newell equations

$$\nabla\left[\frac{\partial F}{\partial k_1^2}\mathbf{k}_1\right]+\nabla\left[\frac{\partial F}{\partial(\mathbf{k}_1\cdot\mathbf{k}_2)}\mathbf{k}_2\right]=0, \tag{2}$$

$$\nabla\left[\frac{\partial F}{\partial k_2^2}\mathbf{k}_2\right]+\nabla\left[\frac{\partial F}{\partial(\mathbf{k}_1\cdot\mathbf{k}_2)}\mathbf{k}_1\right]=0, \tag{3}$$

where F is the Lyapunov functional of the system.

A spatiotemporal dynamics described by Eq. (1) is potential, since Eq. (1) can be written in the variational form

$$\epsilon^2\frac{\partial T}{\partial t}=-\frac{\delta F}{\delta T}, \tag{4}$$

where the Lyapunov functional F is

$$F=\int d^2x\left\{\frac{1}{2}\epsilon^2T^2+\frac{1}{2}[(1+\nabla^2)T]^2+\frac{1}{12}|\nabla T|^4\right\}. \tag{5}$$

Calculating the stationary solutions for rectangles for small ϵ,

$$T=\epsilon a_1e^{i(1+\epsilon K_1)\mathbf{n}_1\cdot\mathbf{x}}+\epsilon a_1e^{i(1+\epsilon K_2)\mathbf{n}_2\cdot\mathbf{x}}+\text{c.c.}+\cdots, \tag{6}$$

and substituting Eq. (6) in Eq. (5), one finds

$$\epsilon^{-4}F=-\frac{\frac{1}{2}\kappa_1^2-\frac{2}{3}[1+2(\mathbf{n}_1\cdot\mathbf{n}_2)^2]\kappa_1\kappa_2+\frac{1}{2}\kappa_2^2}{1-\frac{4}{9}[1+2(\mathbf{n}_1\cdot\mathbf{n}_2)^2]^2}, \tag{7}$$

where $\kappa_1=1-4K_1^2$ and $\kappa_2=1-4K_2^2$. Note that due to the definitions of wave vectors $\mathbf{k}_1$, $\mathbf{k}_2$, $\nabla\times\mathbf{k}_1=\nabla\times\mathbf{k}_2=0$.

Since $k_1=1+\epsilon K_1$, $k_2=1+\epsilon K_2$, the expressions $B(k_1^2,k_2^2,\mathbf{k}_1\cdot\mathbf{k}_2)=\partial F/\partial k_1^2$ and $B(k_2^2,k_1^2,\mathbf{k}_1\cdot\mathbf{k}_2)=\partial F/\partial k_2^2$ are $O(\epsilon^{-1})$, while $C(k_1^2,k_2^2,\mathbf{k}_1\cdot\mathbf{k}_2)=\partial F/\partial(\mathbf{k}_1\cdot\mathbf{k}_2)$ is $O(1)$. Thus, near the threshold (and only there), one can disregard C and write the Cross-Newell equations for rectangles in the leading order as

$$\nabla[B(k_1^2,k_2^2,\mathbf{k}_1\cdot\mathbf{k}_2)\mathbf{k}_1]=0, \tag{8}$$

$$\nabla[B(k_2^2,k_1^2,\mathbf{k}_1\cdot\mathbf{k}_2)\mathbf{k}_2]=0, \tag{9}$$

where (after rescaling)

$$B(k_1^2,k_2^2,\mathbf{k}_1\cdot\mathbf{k}_2)=4K_1\frac{(1-4K_1^2)-(2/3)[1+2(\mathbf{n}_1\cdot\mathbf{n}_2)^2](1-4K_2^2)}{1-\frac{4}{9}[1+2(\mathbf{n}_1\cdot\mathbf{n}_2)^2]^2}, \tag{10}$$

and $B(k_2^2,k_1^2,\mathbf{k}_1\cdot\mathbf{k}_2)$ is obtained from Eq. (10) by replacing 1 by 2 and vice versa, $K_j=\epsilon^{-1}(k_j-1)$. For perfect squares, $\mathbf{n}_1\cdot\mathbf{n}_2=0$ and $C=0$ exactly.

In the case of a disclination, Eqs. (8) and (9) can be represented as a single equation for a function $\mathbf{k}=\nabla\Theta$ defined [in the polar coordinates (r,θ)] in the region $0\leqslant\theta\leqslant4\pi$, such that $\mathbf{k}_1(\theta)\equiv\mathbf{k}(\theta)$, $\mathbf{k}_2(\theta)\equiv\mathbf{k}(\theta+2\pi)$, $0\leqslant\theta\leqslant2\pi$.

A reasonable approximation to the solution of Eqs. (8)–(10) can be found if the nonlinear interaction between rolls in the rectangular pattern is weak so that one can neglect the dependence of $B(k_1^2,k_2^2,\mathbf{k}_1\cdot\mathbf{k}_2)$ on all the arguments except the first one, i.e., to consider $B=B(k_1)$. In this case, a solution to the Cross-Newell equations for rectangles can be considered as a solution for rolls, but defined in a region $0\leqslant\theta\leqslant4\pi$. Following Ref. [3], use the Legendre transformation to obtain the following linear equation:

$$k\frac{\partial}{\partial k}\left[kB(k)\frac{\partial\hat{\Theta}}{\partial k}\right]+\frac{\partial}{\partial k}[kB(k)]\frac{\partial^2\hat{\Theta}}{\partial\phi^2}=0. \tag{11}$$

An appropriate solution of Eq. (11) is $\hat{\Theta}=F_m(k)\cos m\phi$, where

$$k[kB(k)F_m'(k)]'-m^3kB(k)F_m(k)=0. \tag{12}$$

In the case $m=1$ corresponding to a disclination in a roll pattern, Eq. (12) can be solved analytically [3].

A convex disclination in a square pattern, with the topological charge 1/4, corresponds to $m=3$. In this case, an approximate solution of Eq. (12) can be found in the far-field region, $r\gg1$. Indeed, as follows from Ref. [3], the region $r\gg1$ corresponds to rolls with k close to the value k_0 at the boundary of the zigzag instability, where $B(k_0)=0$ (in our case $k_0=1$, and $K_0=0$). Near $k=k_0$,

$$F_m(k)\sim\ln(k_0-k), \tag{13}$$

and does not depend on m. The solution of Eq. (13) in x space is given by $\mathbf{x}=\nabla_{\mathbf{k}}\hat{\Theta}$, which yields

$$r\cos(\theta-\phi)=F_m'(k)\cos m\phi, \tag{14}$$

$$r\sin(\theta-\phi)=-\frac{mF_m(k)}{k}\sin m\phi, \tag{15}$$

where ϕ determines the direction of the vector $\mathbf{k}$. Thus, one gets

$$\theta=\phi+\arctan(\delta\tan m\phi),\quad \delta=-\frac{mF_m(k)}{kF_m'(k)}. \tag{16}$$

In the limit (13) δ is small, so that one obtains fast change of θ near $\phi=(\pi/m)(2n+1)$ (i.e., sectors with nearly straight rolls) and sectors with $\theta=\phi+n\pi$ (i.e., sectors with targets).

For example, an approximate far-field solution corresponding to a convex disclination with the topological charge 1/4 is

$$T=\cos(x\cos\phi_1+y\sin\phi_1)+\cos(x\cos\phi_2+y\cos\phi_2), \tag{17}$$

where

$$\phi_1=\theta,\ 0<\theta<\frac{\pi}{6};\quad \phi_2=\frac{\pi}{2},\ 0<\theta<\frac{\pi}{2};$$

$$\phi_1=\frac{\pi}{6},\ \frac{\pi}{6}<\theta<\frac{7\pi}{6};\quad \phi_2=\theta,\ \frac{\pi}{2}<\theta<\frac{5\pi}{6}; \tag{18}$$

$$\phi_1=\theta-\pi,\ \frac{7\pi}{6}<\theta<\frac{3\pi}{2};\quad \phi_2=\frac{5\pi}{6},\ \frac{5\pi}{6}<\theta<\frac{11\pi}{6};$$

$$\phi_1=\frac{\pi}{2},\ \frac{3\pi}{2}<\theta<2\pi;\quad \phi_2=\theta-\pi,\ \frac{11\pi}{6}<\theta<2\pi.$$

In the far field this pattern is similar to that shown in Fig. 1, but does not contain the disclination core. Similar approximation for a concave disclination with the topological charge $-1/4$ cannot be found within the framework of this approach since the function $\theta(\phi)$ turns out to be nonmonotonic in this case which is unphysical. The approximation used underestimates the role of the interaction between rolls forming the square patterns. Nevertheless, the approximate solution (17), (18) reproduces correctly the basic topological features of the numerical solution shown in Fig. 1.

III. DISCLINATIONS IN HEXAGONAL PATTERNS

In order to study a possibility for a stable disclination to exist in a hexagonal pattern, we have performed numerical simulations of two generic equations known to exhibit hexagonal planforms: *Swift-Hohenberg equation* with a square nonlinearity,

$$\psi_t=\epsilon\psi-(1+\nabla^2)^2\psi+\alpha\psi^2-\psi^3, \tag{19}$$

which is typical of many *potential* systems [25], and *damped Kuramoto-Sivashinsky equation*,

$$\psi_t=\epsilon\psi-(1+\nabla^2)^2\psi-\frac{1}{2}|\nabla\psi|^2, \tag{20}$$

typical of many *nonpotential* systems [26].

Both these equations exhibit, near threshold $\epsilon=0$, the formation of stationary hexagonal patterns. Starting from small-amplitude random noise, one observes the formation of domains filled with hexagons with different orientations, divided by grain boundaries that consist of chains of penta-hepta defects.

We started from small-amplitude initial conditions mimicing a convex and a concave disclination in hexagonal patterns with the topological charges 1/6 and $-1/6$, respectively, discussed above. As a result, the solutions evolved into stable disclination patterns, examples of which are shown in Figs. 3 and 4. Figure 3 shows a convex disclination in a hexagonal pattern with the topological charge 1/6 resulting from Eq. (20). Figure 4 corresponds to a concave disclination in a hexagonal pattern with the topological charge $-1/6$ resulting from Eq. (19). One can see that the structure of the disclinations in hexagonal patterns is similar to that in a square one. It consists of a core that can be considered as a bound state of several penta-hepta defects, and a hexagonal pattern with a certain number of symmetrically located penta-hepta defects around the core. It is important to note that these penta-hepta defects *do not* form domain bound-

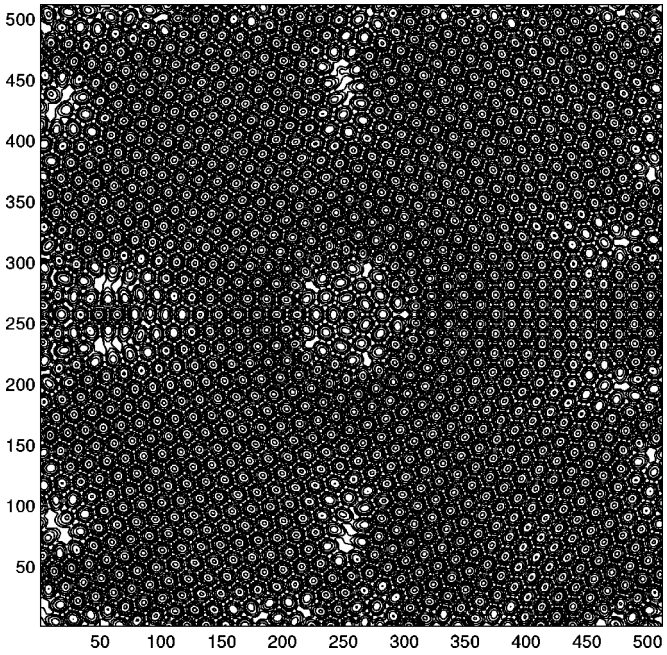

FIG. 3. Stable solution of Eq. (20) with $\epsilon=0.02$, in the form of a convex disclination in a hexagonal pattern, with the topological charge 1/6.

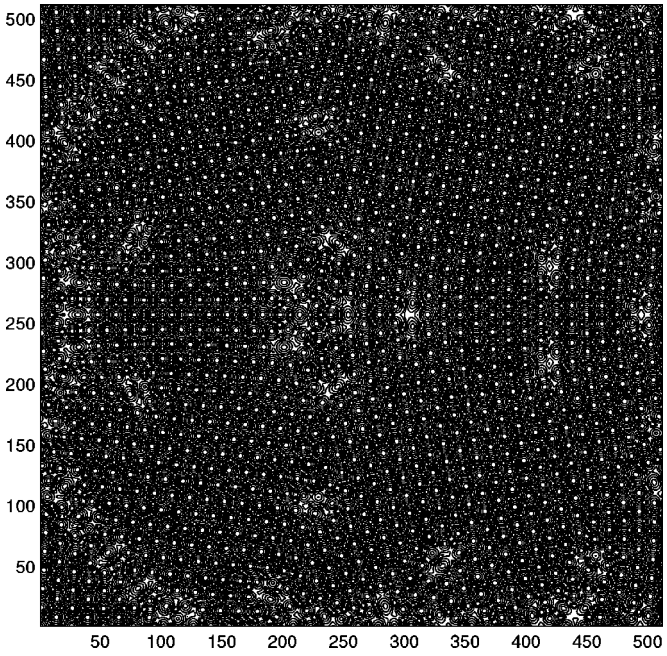

FIG. 4. Stable solution of Eq. (19) with $\epsilon=0.02$, $\alpha=1.0$, in the form of a concave disclination in a hexagonal pattern, with the topological charge $-1/6$.

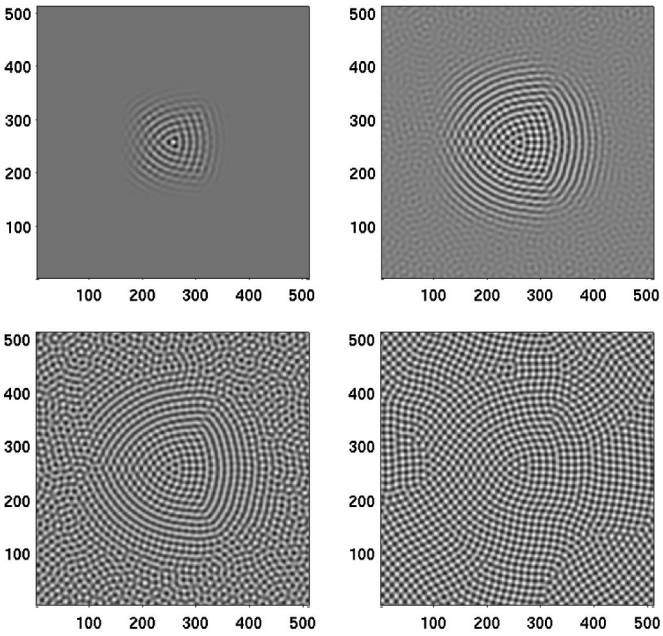

FIG. 5. Nucleation of a disclination in a square pattern—numerical solution of Eq. (1) with $\epsilon^2 = 0.1$.

aries between domains with differently oriented hexagons as is usually the case when a hexagonal pattern evolves from random initial data. Rather, it is possible to go around the core and remain in the same domain of hexagons whose wave vectors rotate continuously by $\pm \pi/3$ for a convex and a concave disclination, respectively.

We have not succeeded in trying to get a qualitative picture of disclination in a hexagonal pattern from Cross-Newell equations for hexagons [24] as we did for a convex disclination in a square pattern, since the interaction (phase correlation) of the systems of rolls forming the hexagonal pattern is crucial and one cannot neglect this interaction in the Cross-Newell equations.

IV. NUCLEATION OF DISCLINATIONS AND THEIR STABILITY

In order to see how robust the disclinations in square and hexagonal patterns are, we have performed the following numerical experiment. We have simulated Eqs. (1), (19), and (20) starting from the initial conditions that had a small-size nucleus of the corresponding disclination pattern with a small amplitude, surrounded by a spatially random field with even smaller amplitude. As a result we have observed the growth of disclination patterns from their nuclei into the random surrounding. Example of this growth is shown in Fig. 5 for the case of a square pattern resulting from Eq. (1). One can see that the disclination structure has grown to a considerable size, while at the periphery of the computational region, domains with differently oriented squares have formed. The established disclination structure coexisting with the domains of squares at its periphery turns out to be stable. The structure resulting from the disclination nucleus in a hexagonal pattern described by Eq. (19) appears to be somewhat different. It evolves into four domains of differently oriented

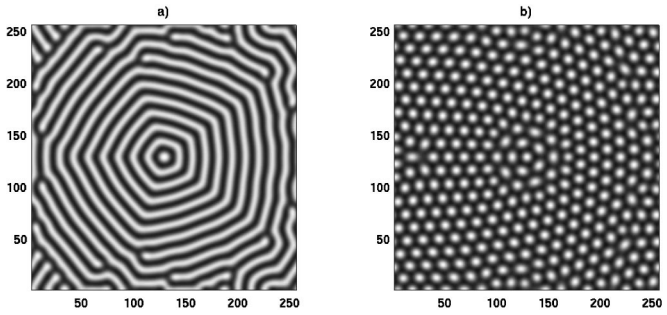

FIG. 6. (a) Concentric roll pattern resulting from a convex disclination with the supercriticality increase from $\epsilon = 0.2$ to $\epsilon = 0.8$. (b) Convex disclination in a hexagonal pattern restored from the concentric roll pattern shown in (a), with the decrease of the supercriticality from $\epsilon = 0.2$ to $\epsilon = 0.8$. Numerical solution of Eq. (19) with $\alpha = 1.0$.

hexagons divided by domain walls composed of the chains of penta-hepta defects. Such structure is different from the disclinations shown in Figs. 3 and 4 in which the orientation of the hexagons is changing *continuously* around the core. This is probably due to the fact that a hexagonal pattern is much less flexible than a square one due to resonance locking of the pattern wave vectors.

Another important question is what happens to disclinations in square and hexagonal patterns with the change of the supercriticality. In the case of a disclination in a square pattern described by Eq. (1), the increase of the supercriticality leads to elimination of dislocations and formation of almost perfect, dislocation-free disclination, see Fig. 1. Formation of dislocation-free disclination can be explained by the fact that farther from the threshold of the short-wave instability generating the square pattern, the band of the excited wave numbers becomes larger which gives more freedom for the local wave vectors of the pattern to adjust themselves to the bending of squares caused by rotation of the disclination structure. With the decrease of the supercriticality, the dislocation-free disclination structure ''cracks'': numerous dislocations appear in it (see Fig. 2).

In the case of hexagonal patterns, the behavior of disclinations with the change of the supercriticality is different. For a disclination in a hexagonal pattern in the potential system described by Eq. (19), we observed that with the increase of the supercriticality, the number of dislocations (penta-hepta defects) remained almost the same. With further increase of the supercriticality, the transition to a roll pattern has been observed which is well known for systems described by the Swift-Hohenberg equation as well as many other pattern-forming systems [25]. The resulting roll pattern is shown in Fig. 6(a) (computations were performed in a smaller domain). It consists of five domains of slightly curved rolls divided by almost dislocation-free domain boundaries and retains the fivefold symmetry of its predecessor—the convex disclination with the topological charge 1/6. It is interesting to note that with the decrease of the supercriticality, the pattern shown in Fig. 6(a) is transformed back to the original disclination structure in a hexagonal pattern shown in Fig. 6(b).

In a nonpotential system described by Eq. (20), the evolution of disclinations in hexagonal patterns differs from that discussed above for the potential system described by Eq. (19). In this case, the increase of the supercriticality leads to a rapid growth of the number of defects that causes the destruction of the disclination structure and the transition to chaos. With the decrease of the supercriticality, the disclination structure is not restored.

V. DISCUSSION AND CONCLUSIONS

In the present work, we have shown that topological defects with fractional topological charges—disclinations—in square and hexagonal patterns can be observed as stationary solutions of several generic evolution equations describing various pattern-forming systems. Stable disclinations in square patterns have topological charges $\pm 1/4$, in hexagonal patterns they have topological charges $\pm 1/6$. Disclinations in square and hexagonal patterns can be observed as a result of the evolution starting from special initial conditions that mimic the disclination structure. We have not observed a spontaneous formation of disclinations in square or hexagonal patterns from random noise. However, a disclination in a square pattern can be formed from a small nucleus that triggers the propagation of the disclination structure through the system. We have also observed that the disclination defects in square and hexagonal patterns are robust in that they are stable within certain interval of the supercriticalities. With the increase of the supercriticality, the behavior of disclinations in square patterns is different from that in hexagonal patterns. In square patterns, the increase of the supercriticality leads to the disappearance of dislocations surrounding the disclination core and to the formation of almost perfect, dislocation-free disclination structure. In hexagonal patterns, it leads to either a destruction of the disclination pattern or to a transition to a concentric roll pattern that retains the symmetry of the disclination. It is important to note that the disclination structure can be restored by the decrease of the supercriticality.

It would be very interesting to systematically study the described disclinations in square and hexagonal patterns in experiments. Although patterns resembling disclination structure were observed in a number of experiments [14,15] and numerical simulations of some reaction-diffusion systems [16–18], we are currently not aware of any systematic experimental investigations of the disclination defects in square or hexagonal patterns. We could suggest that one can try to use Marangoni convection in large Prandtl number fluids as an experimental system in which the disclinations could be observed. This system is known to exhibit both square and hexagonal spatially regular patterns. Moreover, an elegant experimental method of controlling and producing a desired pattern in Marangoni convection by means of a laser radiation has been proposed and tested recently [27].

In order to check the possibility to observe disclinations in Marangoni convection patterns, we have also performed numerical simulation of an evolution equation that describes large-scale Marangoni convection in a thin, large aspect ratio layer of large (infinite) Prandtl number liquid, with nearly thermally insulated top and bottom surfaces [28–30]:

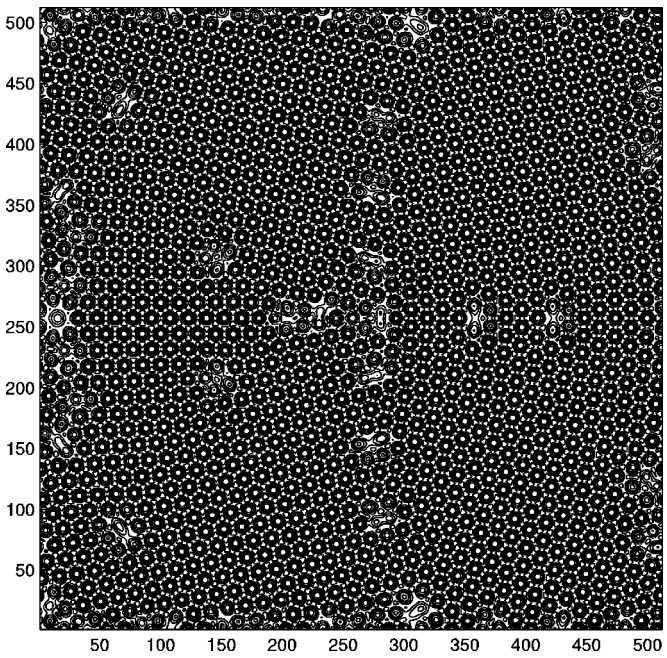

FIG. 7. Disclination in a hexagonal pattern resulting from numerical solution of Eq. (21) with $\beta = 0.98$.

$$\partial_t \Phi + 2\Delta\Phi + \Delta^2\Phi - \nabla\cdot(|\nabla\Phi|^2\nabla\Phi) + \lambda\nabla\cdot(\Delta\Phi\nabla\Phi) + \mu\Delta|\nabla\Phi|^2 + \beta\Phi = 0, \tag{21}$$

where Φ is the temperature field at the free surface of the liquid layer, $\lambda = \sqrt{7}/8, \mu = 3\sqrt{7}/4$ and β is the bifurcation parameter characterizing the heat flux through the liquid layer in the quiescent steady state. The Marangoni convection in a system described by Eq. (21) occurs for $\beta < 1$. One can see that Eq. (21) is similar to Eq. (1) but it contains additional quadratic terms with the coefficients λ and μ that break the $\Phi \to -\Phi$ symmetry and allow for the appearance of a hexagonal pattern typical of Marangoni convection.

Figure 7 shows stable convex disclination structure, with the topological charge 1/6, in a hexagonal pattern resulting from the numerical solution of Eq. (21) starting from small-amplitude initial data that mimic the convex disclination structure. This result may encourage experimentalists to try to obtain stable disclinations in hexagonal patterns in Marangoni convection.

Note that a ''pure'' disclination, without defects except for the core, can be formed only from special initial conditions and in a certain interval of supercriticalities. A more typical situation is characterized by the appearance of dislocations generated by the disclination structure. These dislocations often form chains that mark ''domain walls'' between the regions where the pattern orientation is almost constant. The changes of the pattern orientations are located inside the domain walls. The difference between a pure and a domain wall disclination seems to be quantitative rather than qualitative and could be characterized, for instance, by the mean distance between the dislocations along the domain wall.

ACKNOWLEDGMENTS

This work was supported by Grant No. 9800086 from the Binational U.S.-Israel Science Foundation and by the Fund for the Promotion of Research at the Technion. Part of this work was accomplished during the workshop ''Topology in Condensed Matter Physics'' at the Max Planck Institute in Dresden, Germany. The authors are grateful to the organizers for their hospitality and fruitful atmosphere. We are especially thankful to Michael Monastyrsky for many stimulating discussions.

[1] M. Monastyrsky, *Topology of Gauge Fields and Condensed Matter* (Plenum, New York, 1993).
[2] L.M. Pismen, *Vortices in Nonlinear Fields: From Liquid Crystals to Superfluids, from Non-Equilibrium Patterns to Cosmic Strings* (Oxford University Press, Oxford, 1999).
[3] T. Passot and A.C. Newell, Physica D **74**, 301 (1994).
[4] C. Bowman and A.C. Newell, Rev. Mod. Phys. **70**, 289 (1998).
[5] A.A. Nepomnyashchy, M.G. Velarde, and P. Colinet, *Interfacial Phenomena and Convection* (CRC Press, Boca Raton, 2001).
[6] A. Kudrolli and J.P. Gollub, Physica D **97**, 133 (1996).
[7] P.B. Umbanhowar, F. Melo and H.L. Swinney, Physica A **249**, 1 (1998).
[8] S.H. Davis, *Theory of Solidification* (Cambridge University Press, Cambridge, 2001).
[9] M. Dolnik, A.M. Zhabotinsky, A.B. Rovinsky, and I.R. Epstein, Chem. Eng. Sci. **55**, 223 (2000).
[10] H.J. Pi, S. Park, J. Lee, and K.J. Lee, Phys. Rev. Lett. **84**, 5316 (2000).
[11] T. Ackemann and T. Lange, Appl. Phys. B: Lasers Opt. **72**, 21 (2001).
[12] N.D. Mermin, Rev. Mod. Phys. **51**, 591 (1979).
[13] P.M. Chaikin and T.C. Lubensky, *Principles of Condensed Matter Physics* (Cambridge University Press, Cambridge, 2000).
[14] E. Moses and V. Steinberg, Phys. Rev. A **43**, 707 (1991).
[15] Q. Ouyang and H.L. Swinney, in *Chemical Waves and Patterns*, edited by R. Kapral and K. Showalter (Kluwer, Dordrecht, 1995).
[16] P. Borckmans, A. De Witt, and G. Dewel, Physica A **188**, 137 (1992).
[17] V. Dufiet and J. Boissonade, J. Chem. Phys. **96**, 664 (1992).
[18] B. Pena and C. Perez-Garcia, Phys. Rev. E **64**, 056213 (2001).
[19] A.A. Nepomnyashchy, in Fluid Dyn., in Proceedings of the Perm State Ped. Inst., edited by E.M. Zhukhovitskii [Fluid Dyn. **152**, 53 (1976)].
[20] C.J. Chapman and M.R.E. Proctor, J. Fluid Mech. **101**, 759 (1980).
[21] V.L. Gertsberg and G.I. Sivashinsky, Prog. Theor. Phys. **66**, 1219 (1981).
[22] L.M. Pismen, Phys. Lett. A **116**, 241 (1986).
[23] The fact that the patterns were stationary was checked by monitoring the integral characteristics of the solution, $E = N^{-2}\Sigma_{k=-N/2}^{k=N/2}|\hat{T}_k|^2$, where $\hat{T}_k$ are the Fourier coefficients, and checking that it tends to a constant value.
[24] R.B. Hoyle, Phys. Rev. E **61**, 2506 (2000).
[25] M.C. Cross and P.C. Hohenberg, Rev. Mod. Phys. **65**, 851 (1993).
[26] M. Paniconi and K.R. Elder, Phys. Rev. E **56**, 2713 (1997).
[27] D. Semwogerere and M.F. Schatz, Phys. Rev. Lett. **88**, 054501 (2002).
[28] E. Knobloch, Physica D **41**, 450 (1990).
[29] L. Shtilman and G. Sivashinsky, Physica D **52**, 477 (1991).
[30] A.A. Golovin, A.A. Nepomnyashchy, and L.M. Pismen, Physica D **81**, 117 (1995).